

Supporting Information

Rapid surface reconstruction strategies for oxygen evolution reactions: chemical grafting of MXene quantum dots on Ni-Co layered double hydroxides

Lili Song,^a Xiaoyun Zhang,^a Xinying Du,^a Shifan Zhu,^a Yixue Xu^a and Yuqiao Wang^{*a}

^aResearch Center for Nano Photoelectrochemistry and Devices, School of Chemistry and Chemical Engineering, Southeast University, Nanjing 211189, China

*Corresponding author. E-mail: yqwang@seu.edu.cn (Y. Wang)

Table of Contents

1. Calculated models	3
2. AIMD simulations	3
3. DFT calculations	4
4. Materials	5
5. Catalyst preparation	5
6. Characterization methods	6
7. Electrochemical measurements	6
8. Results and discussions	7-19
9. References	20

1. Calculated models

Calculated models were according to our reported work [1]. Generally, all models derived from Ni(OH)₂ model with a vacuum of 15 Å. The main frame of the MQDs model was constructed using 4 C atoms and 6 Ti atoms. Ni-Co LDH@MQDs was built by Ni(OH)₂ (001) plane and MQDs. MQDs are combined with Ni-Co LDH through Co-O-Ti and Co-O-C bonding in Ni-Co LDH@MQDs. Ni-Co LDH/MQDs was built as a comparison, in which MQDs was placed on the Ni-Co LDH surface without any chemical bond.

2. AIMD simulations

Ab initio molecular dynamic (AIMD) simulations have been carried out at NVT ensemble using Cambridge Sequential Total Energy Package (CASTEP) with the energy cutoff of 400 eV and the convergence of 1.0×10^{-4} eV atom⁻¹. The temperature was maintained at about 300 K using a Nose-Hoover thermostat. The generalized-gradient approximation of Perdew-Burke-Ernzerhof (GGA-PBE) was used for the exchange-correlation interactions [2]. An explicit water model was applied during AIMD simulations. The explicit water model was composed of 20 H₂O molecules to simulate the aqueous solution. A time step of 1 femtosecond (fs) was used for the simulation step size. The 2 picoseconds (ps) trajectory was generated and used for analysis. Center of mass vector (r_{σ}) was average position of the mass point system mass distribution according to the formula:

$$r_{\sigma} = \frac{\sum_i m_i r_i}{M} \quad (1),$$

where m_i was the mass of each component, and r_i represented the vector diameter of each position relative to a fixed point in a system. $M = \sum_{i=1}^n m_i$ meant the total mass of the system. The subsequent structural analysis was applied by VMD software. The root mean squared deviation (RMSD) values

were statistics by the following formula:

$$\text{RMSD} = \sqrt{\frac{\sum_{t=1}^N (x_i - x_i')^2 + (y_i - y_i')^2 + (z_i - z_i')^2}{N}} \quad (2),$$

where the subscript t represented the sequence number of the observation; N was the number of all observations for each monitor for the data set. x_i and x_i' were the x coordinates of the i-th component in the first structure and the second structure, respectively. y and z were similar representations.

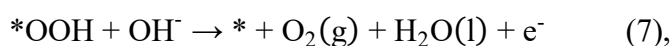
3. DFT Calculations

The spin-polarized density functional theory (DFT) was also implemented in the CASTEP code with the GGA-PBE functional. Calculated structures were selected without H₂O molecules at the specific moment in the trajectory of AIMD simulations. The energy cutoff of 400 eV and Monkhorst–Pack k-mesh of $2 \times 2 \times 1$ were applied. The geometry optimization was carried out before the subsequent calculations of electronic structure. Geometry optimization has been carried out using the Broyden–Fletcher–Goldfarb–Shanno (BFGS) minimization algorithm. The convergence thresholds were set to 1×10^{-5} eV per atom for energy, 0.02 eV/Å for maximum force and 0.02 Å for maximum atomic displacements. The adhesive energy (E_{adh}) was estimated following as:

$$E_{\text{adh}} = E_{\text{T}} - E_{\text{LDH}} - E_{\text{MQDs}} \quad (3),$$

where E_{T} , E_{LDH} and E_{MQDs} were the energies of the overall model, LDH and MQDs models, respectively.

The conventional adsorbate evolution mechanism (AEM) of OER would undergo four primitive reaction in alkaline solution as following [3]:



where * represented the mental active site, *OH, *O and *OOH were the adsorbed intermediates. The Gibbs free energy changes for each OER steps ($\Delta G_1 - \Delta G_4$) can be calculated as shown below:

$$\Delta G = \Delta E + \Delta ZPE - T\Delta S \quad (8),$$

where ΔE is the reaction energy, ZPE is the zero-point energies, and ΔS represents the entropy change.

The barrier of rate-determining step (η) could be determined from free energy differences at each steps as:

$$\eta = \max [\Delta G_1, \Delta G_2, \Delta G_3, \Delta G_4] \quad (9).$$

LDH model at 1200 fs and LDH@MQDs model at 2000 fs without H₂O solvent model were chosen to simulate the reconstituted catalysts and calculate ΔG and η .

4. Materials

All samples were used without further purification. Ni foam (NF) was cleaned by 3M HCl solution and washed by water and ethanol. Ti₃AlC₂ powder was acquired from 11 Technology Co. Ltd. LiF, NiCl₂·6H₂O and CoCl₂·6H₂O reagents were purchased in Sinopharm Group Chemical Reagent Co., Ltd.. The ethanol and ammonia were obtained from McLean Biochemical Technology Co., Ltd.. The hexamethylenetetramine (HMT) were purchased in Aladdin Chemical Reagent Co., Ltd.

5. Catalyst preparation

MXene quantum dots (MQDs) were synthesized from Ti₃AlC₂ according to our reported works [1, 4]. Typically, the few-layer MXene (Ti₃C₂) was prepared by etching and exfoliation of Ti₃AlC₂ with 1 g LiF and 20 mL 9 M HCl solution. MQDs was synthesized by hydrothermal MXene under an alkaline environment (pH = 9).

Ni-Co LDH@MQDs electrocatalyst was prepared by hydrothermal method using reaction solution and a treated NF (3 × 4 × 0.15 cm³) at 100 °C for 8 h. The reaction solution in 40 mL H₂O included MQDs solution (20 mL, 0.5 mg mL⁻¹), NiCl₂·6H₂O (2 mmol) and CoCl₂·6H₂O (4 mmol)

and HMT (1.6 g). As a comparison, pure Ni-Co LDH was prepared by the same methods without MQDs.

Ni-Co LDH/MQDs with the electrostatic bonding was synthesized by Ni-Co LDH and MQDs. Specially, Ni-Co LDH on NF, 20 mL MQDs solution and 40 mL H₂O were put into a 100 mL autoclave. The autoclave was kept at 100 °C for 8 h. Ni-Co LDH/MQDs on NF could be obtained by washing and drying at 60 °C in a vacuum. The load was about 2 mg cm⁻².

6. Materials characterization

X-ray diffraction (XRD) patterns were conducted using an Ultima IV at Cu-K α radiation. Scanning electron microscopy (SEM) was performed on a Hitachi S-4800 instrument. Transmission electron microscopy (TEM), scanning transmission electron microscopy (STEM) and corresponding the energy-dispersive X-ray spectroscopy (EDS) elemental mappings were characterized on a Talos F200X equipment. The X-ray photoelectron spectroscopy (XPS) was collected by a Thermo Scientific K-Alpha spectrometer. Photoluminescence measurements were carried out on a Fluoromax-4 device.

7. Electrochemical measurements

All electrochemical measurements were carried out by a CHI 760E electrochemical workstation in 1.0 M KOH. Prepared catalysts on NF, graphite rod and saturated calomel electrode (SCE) were used as the working electrode counter electrode and reference electrode, respectively. The measured potentials were calibrated to a reversible hydrogen electrode (RHE) according to the Nernst equation: $E(\text{V vs. RHE}) = E(\text{V vs. SCE}) + 0.059 \times \text{pH} + 0.241$. Cyclic voltammetry (CV) and linear sweep voltammetry (LSV) curves were employed to investigate catalytic activities of various electrodes with a scan rate of 2 mV s⁻¹. All the LSV curves were corrected with iR-compensation (90 %). The electrochemically active surface area (ECSA) of the catalysts was evaluated by comparing the double-layer capacitance (C_{dl}) under a potential window without redox reactions (1.205 V~ 1.305 V vs. RHE). Electrochemical impedance spectroscopy was performed at the overpotential of 10 mA cm⁻² in the

frequency range from 0.01 Hz to 100 kHz with AC amplitude of 5 mV.

8. Results and discussions

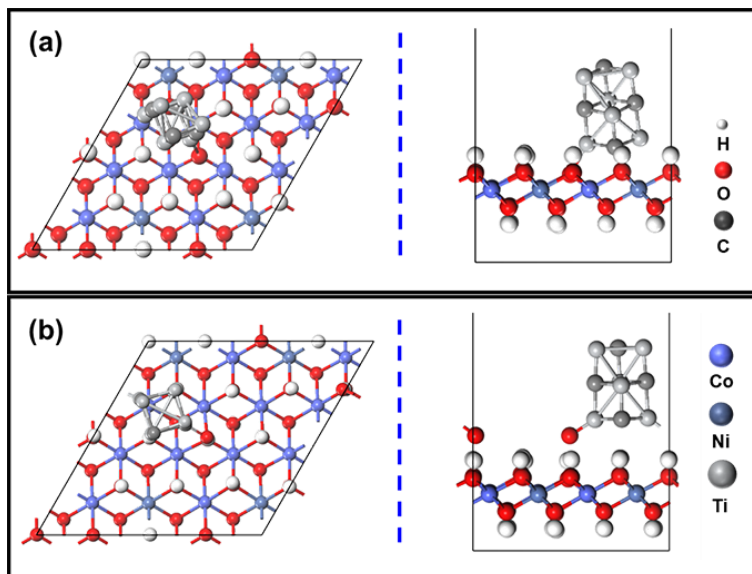


Fig. S1. The top and side views of (a) Ni-Co LDH@MQDs and (b) Ni-Co LDH/MQDs models.

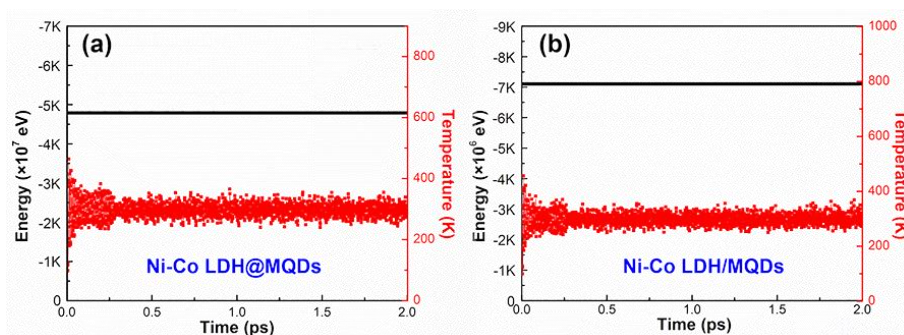


Fig. S2. Oscillations of energy and temperature of Ni-Co LDH@MQDs and Ni-Co LDH/MQDs, respectively.

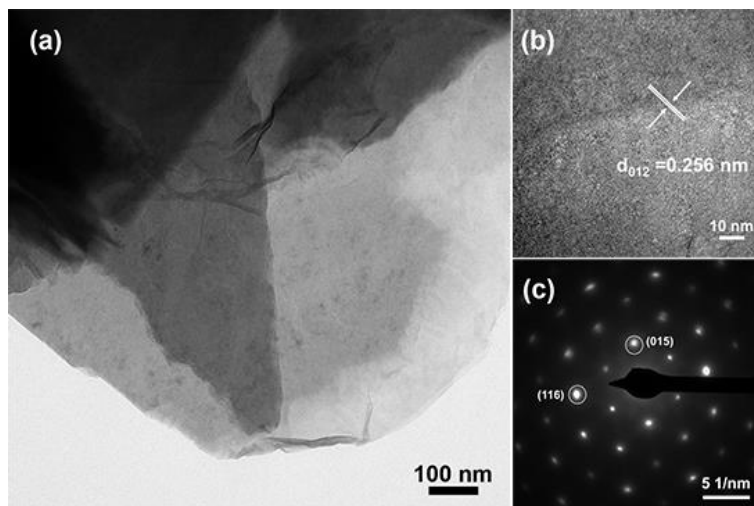


Fig. S3. Ni-Co LDH: (a) TEM image, (b) HRTEM image and (c) SAED pattern.

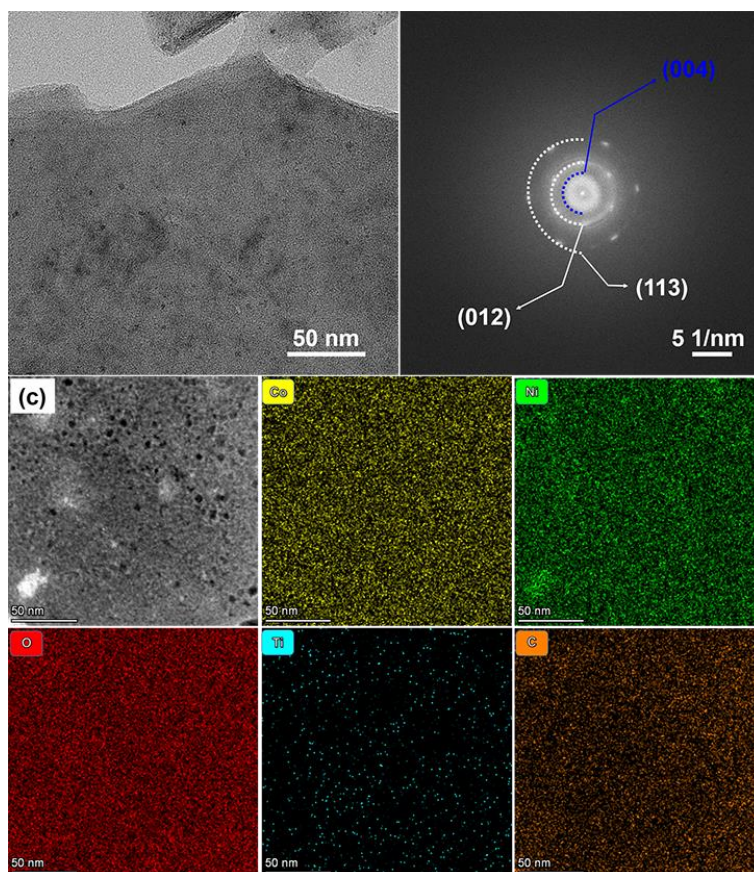


Fig. S4. Ni-Co LDH/MQDs: (a) TEM image, (b) FFT pattern and (c) STEM image and elemental distribution images of Co, Ni, O, Ti and C.

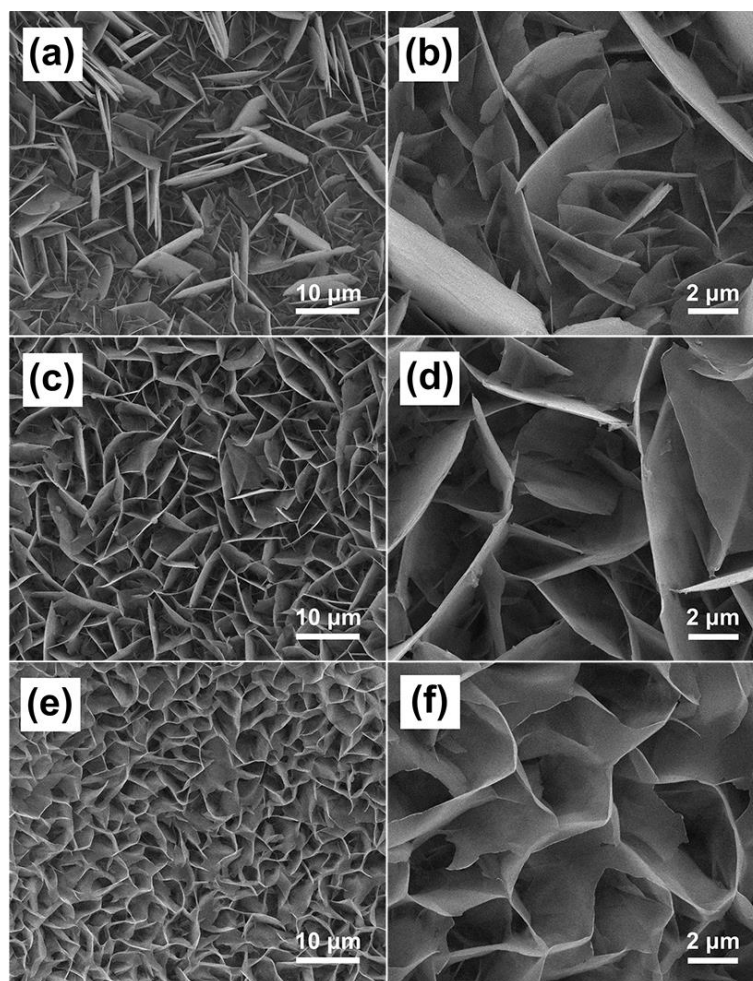


Fig. S5. SEM and enlarged SEM images for (a, b) Ni-Co LDH, (c, d) Ni-Co LDH/MQDs and (e, f) Ni-Co LDH@MQDs catalysts.

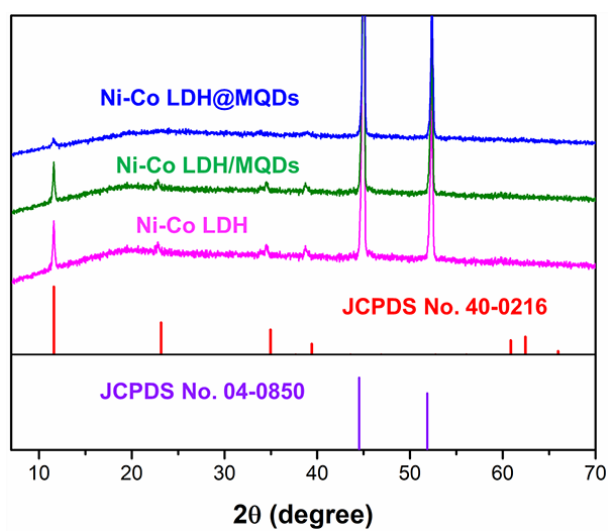


Fig. S6. XRD patterns of as-prepared electrocatalysts.

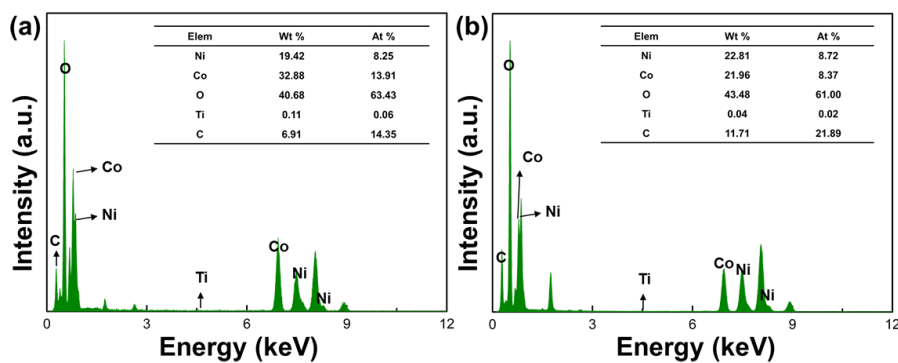


Fig. S7. EDS spectra and the element contents: (a) Ni-Co LDH@MQDs and (b) Ni-Co LDH/MQDs.

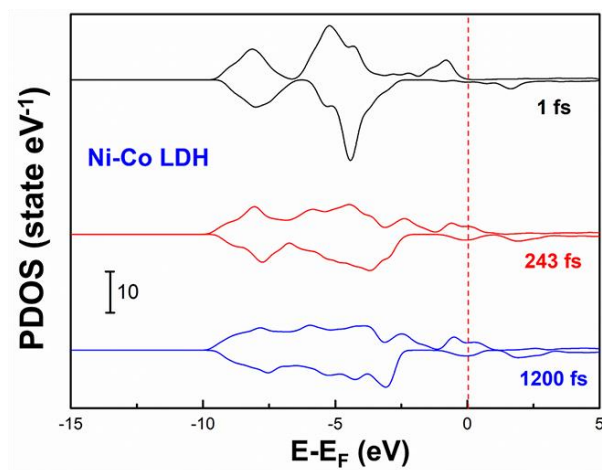


Fig. S8. PDOS curves of the surface oxygen atoms at special simulation moments in Ni-Co LDH.

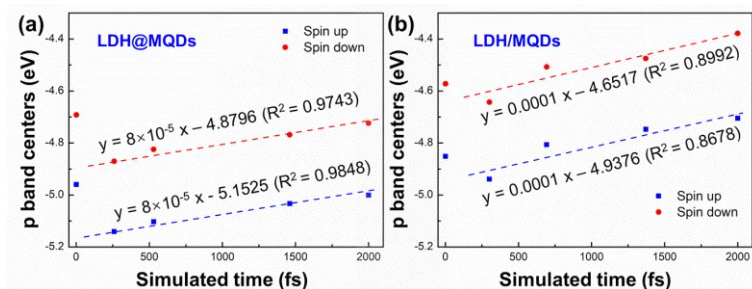


Fig. S9. Calculated p-band centers of surface oxygen atoms for the selected moments in (a) LDH@MQDs and (b) LDH/MQDs.

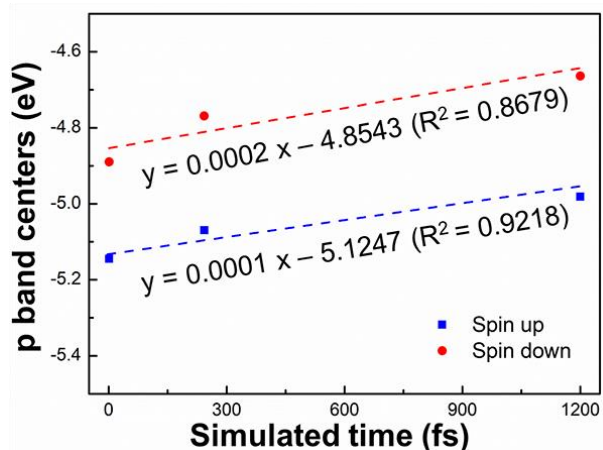


Fig. S10. Calculated p-band center of surface oxygen atoms for the selected moments in LDH.

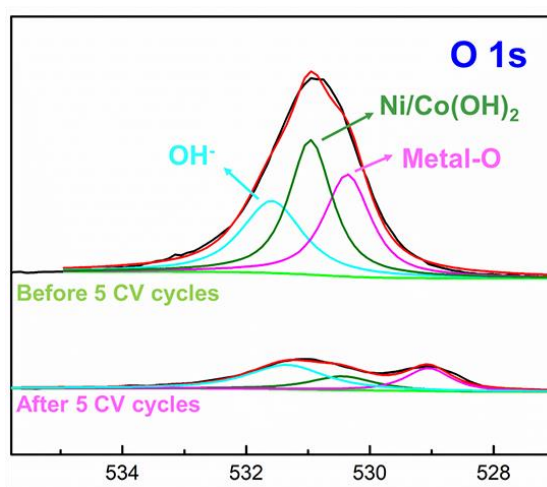


Fig. S11. High-resolution XPS spectra of O 1s in Ni-Co LDH before and after 5 CV cycles.

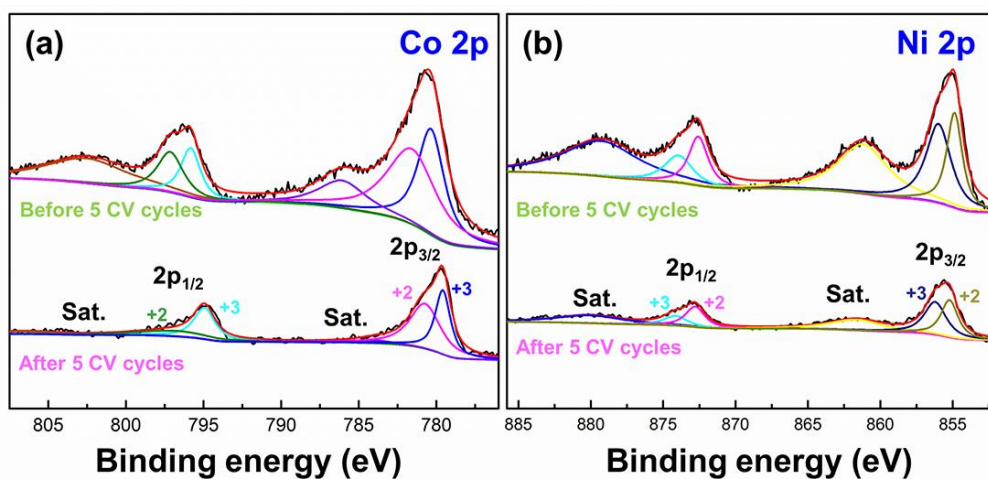


Fig. S12. High-resolution XPS spectra of (a) Co 2p and (b) Ni 2p in Ni-Co LDH before and after 5 CV cycles.

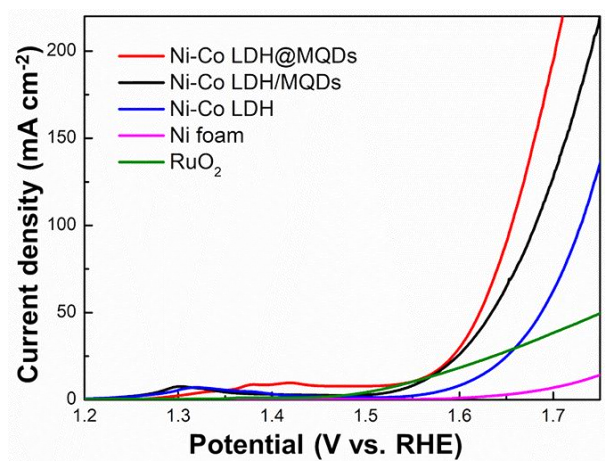


Fig. S13. LSV curves for the prepared catalysts.

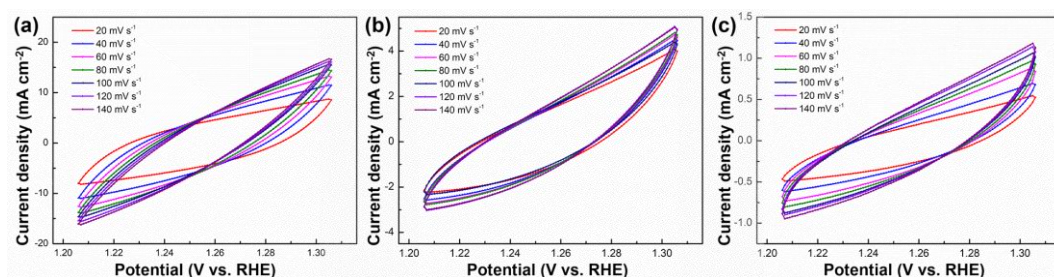


Fig. S14. CV curves of (a) Ni-Co LDH, (b) Ni-Co LDH/MQDs and (c) Ni-Co LDH@MQDs catalysts at different scan rates in a non-faradic region (1.205 V - 1.305 V vs. RHE).

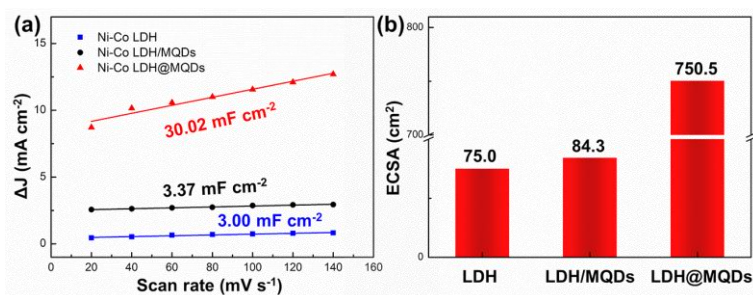


Fig. S15. As-prepared electrocatalysts: (a) C_{dl} values and (b) ECSA values.

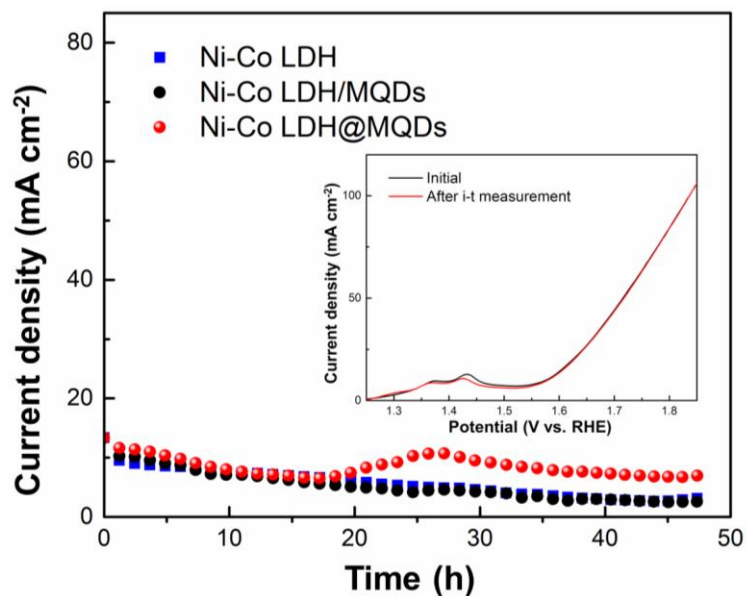


Fig. S16. Potentiostatic i-t curves of prepared catalysts (Inset: LSV plots without IR-compensation of Ni-Co LDH@MQDs before and after 48h tests).

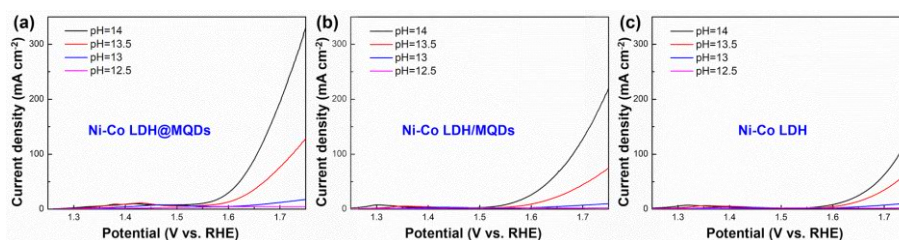


Fig. S17. LSV with 90% IR compensation of (a) Ni-Co LDH, (b) Ni-Co LDH/MQDs and (c) Ni-Co LDH@MQDs scanned in KOH ($\text{pH} \approx 12.5 - 14$) at a scan rate of 2 mV s^{-1}

Table S1. The fitted positions of peaks in XPS data before and after 5 CV cycles.

		LDH@MQDs/eV		LDH/MQDs/eV		LDH/eV	
		Before	After	Before	After	Before	After
	Metal-O	530.36	530.40	530.23	530.62	530.35	529.05
O 1s	Ni/Co(OH)₂	530.93	531.11	530.83	531.15	530.96	530.44
	OH⁻	531.53	531.94	531.47	531.74	531.58	531.34
Co 2p	+2	780.33	779.66	780.22	780.25	780.35	779.59
	2p_{3/2}						
	+3	781.94	780.70	781.40	781.40	781.59	780.73
	2p_{1/2}						
	+2	796.02	795.28	795.90	795.73	795.82	794.94
	+3	797.28	797.08	797.33	796.94	797.13	796.83
Ni 2p	+3	854.99	855.10	854.86	855.29	854.87	855.22
	2p_{3/2}						
	+2	856.04	856.06	855.89	856.31	855.97	856.20
	2p_{1/2}						
	+3	872.24	872.61	872.40	872.92	872.57	872.78
	+2	873.43	873.76	873.62	874.08	873.94	874.14
C 1s	C-O	286.21	285.02	285.98	285.08	/	/
	C=O	288.27	288.63	288.39	288.83	/	/

Table S2. The content ratios of Co^{3+} to Co^{2+} ($\text{Co}^{3+}/\text{Co}^{2+}$) and Ni^{3+} to Ni^{2+} ($\text{Ni}^{3+}/\text{Ni}^{2+}$) before and after 5 CV cycles.

	Before 5 CV cycles		After 5 CV cycles	
	$\text{Co}^{3+}/\text{Co}^{2+}$	$\text{Ni}^{3+}/\text{Ni}^{2+}$	$\text{Co}^{3+}/\text{Co}^{2+}$	$\text{Ni}^{3+}/\text{Ni}^{2+}$
LDH	1.00	0.89	1.07	1.09
LDH/MQDs	1.20	0.71	1.86	0.77
LDH@MQDs	1.29	0.58	1.78	1.12

Table S3. OER performance of various electrocatalysts.

Electrocatalysts	Overpotential @ 10 mA cm ⁻² (mV)	Overpotential @ 20 mA cm ⁻² (mV)	Overpotential @ 50 mA cm ⁻² (mV)	Tafel slope (mv dec ⁻¹)
Ni-Co LDH@MQDs	316	353	392	79
Ni-Co LDH/MQDs	328	358	405	83
Ni-Co LDH	379	410	458	105
Commercial RuO₂	319	370	522	N/A

Ni foam	495	547	N/A	N/A
---------	-----	-----	-----	-----

Table S4. OER performance of related LDH-based catalysts.

Electrocatalysts	Substrate	Overpotential	Tafel slope (mv dec ⁻¹)	Ref.
Ni-Co LDH@MQDs	Ni foam	316 mV@ 10 mA cm ⁻²	79	This work
NiFe-LDH/NGF	Glassy carbon	337 mV@ 10 mA cm ⁻²	45	[5]
Exfoliated Ni-Co LDH	Glassy carbon	330 mV@ 10 mA cm ⁻²	41	[6]
CoM LDH	Glassy carbon	> 400 mV@ 10 mA cm ⁻²	N/A	[7, 8]
NiM LDH	Glassy carbon	> 350 mV@ 10 mA cm ⁻²	N/A	[7, 8]
NiFe-LDH/RGO	Glassy carbon	273 mV@ 30 mA cm ⁻²	49	[9]
NiFe-LDH	Glassy carbon	302 mV@ 10 mA cm ⁻²	40	[10]

Table S5. OER performance of reported catalysts.

Electrocatalysts	Electrolyte	Overpotential @ 10mA cm⁻² (mV)	Tafel slope (mv dec⁻¹)	Ref.
Ni-Co LDH@MQDs	1 M KOH	316	79	This work
CoN_x/G	1 M KOH	359	81	[11]
Co/G	1 M KOH	396	87	[11]
Co/NG	1 M KOH	> 500	178	[11]
CoTe₂@NCNTFs	1 M KOH	330	83	[12]
NiCoP/C nanoboxes	1 M KOH	330	96	[13]
ZIF-67 MPs	1 M KOH	427	130.52	[14]
ZIF-67@Co-Fe PBA YSMPs	1 M KOH	288	80.07	[14]
Commercial RuO₂	1 M KOH	367	82.61	[14]
2.5 Fe-NiCoP/PBA HNCs	1 M KOH	290	70	[15]
Co₃O₄/CNTs	1 M KOH	342	72	[16]

CoP NFs	1 M KOH	323	49.6	[17]
CoP NCs	1 M KOH	354	59.3	[17]

Table S6. The fitted parameters of the equivalent circuit based on Nyquist plots.

Catalysts	R_s (Ω)	R₁ (Ω)	n₁	R₂ (Ω)	n₂
LDH@MQDs	1.437	1.429	0.878	0.308	0.485
LDH/MQDs	0.328	1.802	0.989	2.107	0.713
LDH	1.652	0.120	0.712	4.223	0.816

9. References

1. L. Song, S. Zhu, L. Tong, W. Wang, C. Ouyang, F. Xu and Y. Wang, *Mater. Adv.*, 2021, **2**, 5622–5628.
2. S. Grimme, J. Antony, S. Ehrlich and H. Krieg. *J. Chem. Phys.*, 2010, **132**, 154104.
3. Z. Chen, R. Zheng, M. Graś, W. Wei, G. Lota, H. Chen and B. J. Ni, *Appl. Catal. B*, 2021, **288**, 120037.
4. W. Wang, D. Jiang, X. Chen, K. Xie, Y. Jiang and Y. Wang, *Appl. Surf. Sci.*, 2020, **515**, 145982.
5. C. Tang, H. Sen Wang, H. F. Wang, Q. Zhang, G. L. Tian, J. Q. Nie and F. Wei, *Adv. Mater.*, 2015, **27**, 4516–4522.
6. Y. Wang, D. Yan, S. El Hankari, Y. Zou and S. Wang, *Adv. Sci.*, 2018, **5**, 1800064.
7. F. Dionigi, Z. Zeng, I. Sinev, T. Merzdorf, S. Deshpande, M. B. Lopez, S. Kunze, I. Zegkinoglou, H. Sarodnik, D. Fan, A. Bergmann, J. Drnec, J. F. de Araujo, M. Gliech, D. Teschner, J. Zhu, W. X. Li, J. Greeley, B. Roldan Cuenya, and P. Strasser, *Nat. Commun.*, 2020, **11**, 2522.
8. F. Dionigi, J. Zhu, Z. Zeng, T. Merzdorf, H. Sarodnik, M. Gliech, L. Pan, W. Li, J. Greeley and P. Strasser, *Angew. Chem. Int. Ed.*, 2021, **60**, 14567–14578.
9. J. Shen, P. Zhang, R. Xie, L. Chen, M. Li, J. Li, B. Ji, Z. Hu, J. Li, L. Song, Y. Wu and X. Zhao, *ACS Appl. Mater. Interfaces.*, 2019, **11**, 13545-13556.
10. M. Yu, E. Budiayanto and H. Tüysüz, *Angew. Chem. Int. Ed.*, 2022, **61**, e202103824.
11. Q. Huang, B. Wang, S. Ye, H. Liu, H. Chi, X. Liu, H. Fan, M. Li, C. Ding, Z. Li and C. Li, *ACS Catal.*, 2022, **12**, 491–496.
12. X. Wang, X. Huang, W. Gao, Y. Tang, P. Jiang, K. Lan, R. Yang, B. Wang and R. Li, *J. Mater. Chem. A*, 2018, **6**, 3684–3691.
13. P. He, X. Y. Yu and X. W. D. Lou, *Angew. Chem. Int. Ed.*, 2017, **56**, 3897–3900.
14. J. Shi, F. Qiu, W. Yuan, M. Guo and Z. Lu, *Chem. Eng. J.*, 2021, **403**, 126312.
15. D. Li, C. Liu, W. Ma, S. Xu, Y. Lu, W. Wei, J. Zhu and D. Jiang, *Electrochim. Acta.*, 2021, **367**, 137492.
16. K. Lu, T. Gu, L. Zhang, Z. Wu, R. Wang and X. Li, *Chem. Eng. J.*, 2021, **408**, 127352.
17. L. Ji, J. Wang, X. Teng, T. J. Meyer and Z. Chen, *ACS Catal.*, 2019, **10**, 412-419.

